IEICE Proceeding Series

Stochastic resonance in the peripheral auditory system

Florian Gomez, Stefan Martignoli, Ruedi Stoop

Vol. 2 pp. 417-420
Publication Date: 2014/03/18
Online ISSN: 2188-5079

2013 International Symposium on Nonlinear Theory and its Applications
NOLTA2013, Santa Fe, USA, September 8-11, 2013

Stochastic resonance in the peripheral auditory system

Florian Gomez[†], Stefan Martignoli[†,‡], and Ruedi Stoop[†]

†Institute of Neuroinformatics, University and ETH Zurich
Winterthurerstrasse 190, 8057 Zurich, Switzerland
‡Department of Mathematics, University of Applied Sciences HSR Rapperswil
Oberseestrasse 10, 8640 Rapperswil, Switzerland
Email: fgomez@ini.phys.ethz.ch, smartign@hsr.ch, ruedi@ini.phys.ethz.ch

Abstract—The understanding and modeling of the peripheral hearing system (cochlea, outer and inner hair cells, auditory nerve and the lowest auditory nuclei) is a biophysics and scientific computing challenge. We have developed such a framework with real-time capacity. The model not only allows for a selective tuning towards desired sound components in cocktails of sounds. It, moreover, demonstrates the complicated change the auditory signal undergoes on its way higher up the auditory pathway. One intriguing property of the model is that it exhibits that the auditory pathway uses stochastic resonance, in order to relay the sound information gathered and generated in the cochlea higher up the auditory pathway in the most faithful way. Nontrivial manifestations of stochastic resonance in biology are extremely rare. In our case, the effect seems to express an explicit desire of the biological system to maintain artificial auditory signal components that are generated by the cochlear nonlinearities, the purpose of which at the moment we can only speculate on. A side-effect is, however, that it explains the surprising large degree of noise that we find in the firing of the neurons of the auditory nerves.

1. Introduction

Among all human sensors, the hearing system has withstood an accurate physical description the longest. Recent progress has revealed that hearing phenomena previously believed to be located in the CNS are the consequences of the nonlinear physics properties of the cochlea [1]. Here, in continuation of this work, we describe what physics principles are used to generate the biophysical and psychoacoustic hearing information along the hearing pathway up to the auditory nerve. From a physics point of view, the transduction of external sound towards the CNS involves three components: The hearing sensor (cochlea), the attached inner hair cells (IHC), and the auditory nerve neurons (ANN). In the following, we will present exclusively data from our software implementation of the compound device (for consistency), though our hardware implementation yields essentially indistinguishable results. Our *Hopf cochlea* [2, 3, 1, 4] serves as the hearing sensor. The auditory input signal first passes a Hilbert transform to obtain the dimensionality required to drive Hopf systems that act as nonlinear amplifiers. The Hopf cochlea faithfully reflects mammalian sound processing (and beyond [5]): Strong enhancement of weak and compression of strong input signals, by large gain active nonlinear input amplification. Phenomena emerging from this nonlinear behavior, like combination tone and two-tone suppression laws, provide important tests for corroborating the validity of the approach.

Our Hopf cochlea has an intrinsic mesoscopic design: The frequency axis is discretized into a set of sections, each section modeling the nonlinear amplification process along a region of the basilar membrane. The discretization is flexible; here, one section covers approximately a quarter octave. Each section is endowed with properties of the passive hydrodynamic behavior and an active Hopf amplifier. The active part implements the Hopf normal form [6]

$$\dot{\mathbf{z}} = (\mu + j)\omega_c \mathbf{z} - \omega_c |\mathbf{z}|^2 \mathbf{z} - \omega_c \mathbf{F}(t),\ \mathbf{z} \in \mathbb{C}. \qquad (1)$$

Here, the vectors of the input $\mathbf{F}(t)$ and output $\mathbf{z}$ are complex variables (j is the imaginary unit), and $f_c = \omega_c/2\pi$ is the characteristic frequency of the section. μ is the tunable parameter that defines each section's distance from the Hopf bifurcation point at $\mu = 0$. Each section is composed of a Hopf amplifier followed by a section-specific 6th-order Butterworth (low pass) filter modeling the viscous fluid losses. For the results presented below, we use the parameters as in Refs. [1, 4]; we will display the responses of the frequency channels $f_c = 1760$ Hz and $f_c = 440$ Hz. The responses of this cochlea are in perfect agreement with biophysical measurements, for both amplitude and phase of the propagating signal [4].

We have complemented this cochlea by *inner hair cells* IHC, where the cochlear membrane state $V_{Co}(t)$ is linearly relayed to displacements u of the IHC cilia according to $u(t) = 20 \cdot 10^{-9} \cdot V_{Co}(t)$, which affect the IHC voltage V_{IC} according to the standard IHC model [7] (for the equations see the original article; we use the model's standard *in vivo* parameters). The dynamical role of IHC is to half-wave rectify and slightly compress the signal: on top of a frequency-dependent DC component, the output has now a slightly low-pass filtered AC component [7].

The IHC signal feeds into the ANN. Biological ANN show widely divergent response properties. At first view, their extreme noisiness seems to work against their ability to

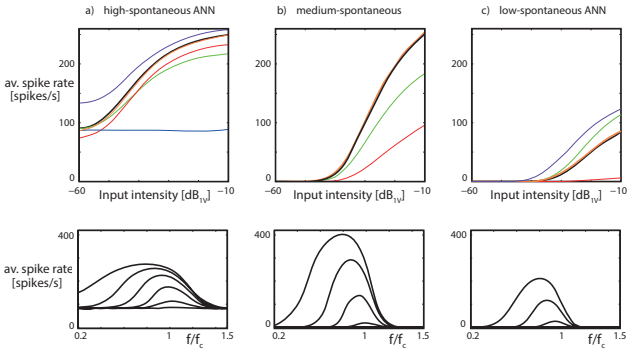

Figure 1: ANN response classes. Upper panel: Black lines from the standard parameter values of Table 1. Colored lines are from the bracketed values of parameter A (red), B (green), σ (purple) and τ_σ (orange). Spontaneous rates: $B = 0$ (blue). Lower panel: Corresponding ANN spike rates ($f_c = 1760$ Hz). Cochlear information is relayed into ANN spike rates that take care of different dynamic ranges, but preserve the essentials of the cochlear signal (here on linear spike rate scale, in Fig. 2 last row on logarithmic scale).

convey precise hearing that crucially depends on precise timing and frequency. Our study will, however, reveal that the opposite is true and that there is a beneficial effect of noise. Biological ANN fall into two main classes [8, 9, 10]: High spontaneous ANN fire at a high rate even in the absence of input, whereas ANN from the other class require substantial input for firing, with a tendency to phase-lock onto the signal involving a substantial degree of jitter. On a finer level, this second class is often divided into a medium- and a low-spontaneous ANN that mainly differ in their distances to firing threshold and maximal spike rate [10, 11]. In our approach, the transmission from IHC to ANN is concatenated into a time-sampled ANN input $I(t_n)$. This input is complemented by a strong contribution of noise, strongly correlated in time, to reflect the nature of the neurotransmitter release. As a result, we chose $I(t_n)$ to have the form

$$I(t_n) = A + B \cdot 20 \cdot (V_{IC}(t_n) - V_{IC,rest}) + \sigma \cdot \xi(t_n), \qquad (2)$$

where constant A has the effect of a firing threshold and where B scales IHC voltage to the evoked ANN current. ξ is exponentially correlated synaptic noise of intensity σ, independent for each transmission channel (we use the algorithm of Ref. [12], with a correlation time constant τ_σ. Our paradigm would, however, work equally well with white noise, though at a synapse, this would be less plausible). With this form of $I(t_n)$, noise can trigger spontaneous ANN firing at low firing thresholds even in the absence of (other) input. The correlation time of the noise was determined by matching our approach with biological data [13]. Following the conjecture [14] that the distinguished postsynaptic potentials (sub-threshold for low-spontaneous, and super-threshold for high-spontaneous ANN) are the consequence of the different biological wiring, we use $A = 0$ for the high- and $A = -0.2$ for the low- and medium spontaneous classes, and ensure that low- and medium-spontaneous ANN need, in addition to the continuous part of $I(t)$, a noise contribution $\xi(t)$ to cross the spiking threshold. For appropriate parameter values, the membrane potential x_n of Rulkov's spike-afterhyperpolarization neuron model [15]

	A	B	γ_{hp}	σ	τ_σ
$Hs:$	$0(-0.02)$	$1(0.8)$	0.97	0.1(0.2)	3(5)
$Ms:$	$-0.2(-0.25)$	$1.25(1.15)$	0.5	0.06(0.04)	3(5)
$Ls:$	$-0.2(-0.25)$	$1.05(1.15)$	0.5	0.04(0.06)	3(5)

Table 1: Parameter values of the three ANN classes. Values in brackets correspond to the parameter variations in Fig. 1 exhibited by colored lines.

$$x_{n+1} = \begin{cases} (v := y^{rs} + \beta^{hp} y_n + \beta^e I_n) \\ \frac{\alpha}{1-x_n} + v, \;\; x_n \le 0, \\ \alpha + v, \;\; 0 < x_n < \alpha + v; \;\; x_{n-1} \le 0, \\ -1, \;\; x_n \ge \alpha + v; \;\; \text{or } x_{n-1} > 0, \end{cases} \qquad (3)$$

$$y_{n+1} = \gamma^{hp} y_n - \begin{cases} g^{hp} & \text{if } n\text{-th iteration spiked,} \\ 0 & \text{otherwise,} \end{cases}$$

reproduces the characteristic biological spike trains of the different ANN classes indistinguishably from biology. In this model, y_n is a slow hyperpolarizing current, whereas constant y^{rs} defines the resting potential. I_n represents the external driving current. A spike is generated every time x_n attains its maximum value. Spike frequency and spike strength are controlled by the parameters γ^{hp} and g^{hp}. Upon constant input current, the nonlinear function $x_{n+1} = f(\ldots)$ generates a (jittered) limit-cycle behavior. We use parameter values $\alpha = 3.8$, $y^{rs} = -2.9$, $b^{hp} = 0.5$, $g^{hp} = 0.1$ and $b^e = 0.1$ [15] and modify the original timescale by a factor of ten. This yields a sampling rate of 20 kHz that is maintained throughout the compound system, to account for very fast spiking ANN, and generates an almost linear I-f curve [15]. The typical responses of the three ANN classes (cf. [11]) are reproduced in Fig. 2 by stimulating the map with a single tone at f_c for varying input intensity at one of the three standard parameter sets of Table I (black lines). The colored lines contained in the figures demonstrate that all biologically observed profiles can be generated by the model by sweeping the parameters across intervals around the standard values, without ever running into non-physiological responses.

2. Compound model performance:

Across the different stages of the compound system, the cochlear information is essentially preserved. In Fig. 2, the outputs of the Hopf cochlea (top panel), of the IHC (second and third panels) and of the ANN (lowest panel) are shown,

for two frequency channels. For the experiments, a single tone with fixed amplitude was fed into the Hopf cochlea, sliding input frequencies from $0.2\,f_c$ to $1.5\,f_c$. To cover an input range from -60 dB$_{1V}$ up to 0 dB$_{1V}$, the experiment was repeated in steps of 10 dB. At the Hopf cochlea, the amplitude of the (single tone)-oscillation was measured; at the IHC, the amplitudes of both the AC- and the DC-components were measured. At the level of the ANN, the amplitude of the neuronal firing was measured in terms of spike rates.

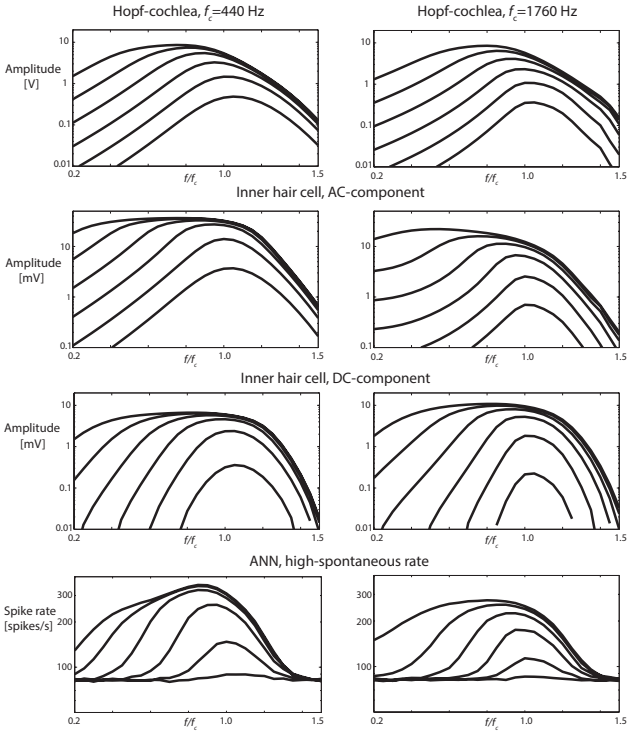

Figure 2: Output amplitudes (logarithmic scale) as a function of input frequency (linear scale). Lines represent constant cochlear input intensities, from -60 dB$_{1V}$ = 1 mV (lowest) to -10 dB$_{1V}$ (uppermost line), in steps of 10 dB. The characteristic cochlear information is preserved across the different stages of transcription.

From these measurements it follows that all essential features of the mammalian cochlea are faithfully reproduced. The most prominent easily verifiable ones are the strong amplification of faint sounds, compressive nonlinearity of exponent one-third, left-shift of the response peaks upon an increase of the input amplitude and characteristic broadening of particularly the low frequencies for low input amplitudes [6, 2, 1, 4]. IHC low-pass filtering (c.f. Fig. 2 f_c = 1760 Hz) is accompanied by strong input sound compression (c.f. f_c = 440 Hz) [7]. Upon feeding the IHC signal into the ANN, spikes recover the original quality of the cochlear response (Fig. 2, last row, for high-spontaneous ANN). High-spontaneous neurons show a quicker saturation for loud sounds, low-spontaneous neurons only respond above an input intensity of ~ -30 dB, thereby taking care of different dynamic ranges. On the linear spike rate scale, each class faithfully transmits the essentials of the Hopf cochlea output (Fig. 1, last panel vs. Fig. 2, first panel), but each on a dynamic range of its own. On the typical dynamic ranges transmitted, all three neuron classes fully retain the cochlear information (Fig. 1). Generated tuning curves (an often used alternative to characterize auditory response by iso-intensity tuning curves) for BM cochlea motion and for the different ANN are very similar. Moreover, they agree with the biological data [16, 10] that serve as the guideline for a faithful transduction from cochlea to CNS [16].

3. Suprathreshold stochastic resonance

To what extent presence of noise plays a distinguished role in achieving this performance we shall exhibit by a pitch-shift experiment [17, 18]. If an AM sound with f_{car} = 850 Hz and f_{mod} = 200 Hz is fed into the cochlea (at an amplitude of $-17dB_{1V}$), this corresponds to a pitch-shift experiment with f_0 = 200 Hz, k = 4 and δf = 50 Hz, generating a *perceived pitch* $f_p = f_0 + \frac{\delta f}{k}$ = 212.5 Hz, equivalent to a period of 4.7 [ms] [17, 18, 19, 1].

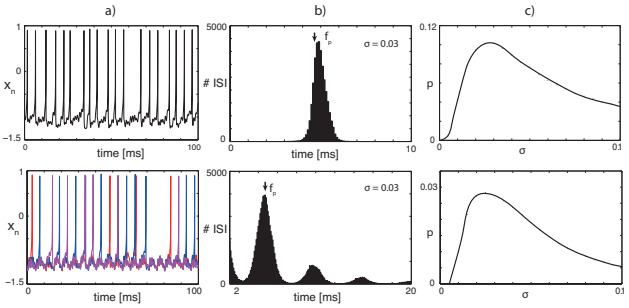

Figure 3: Suprathreshold stochastic resonance of high/low-medium spontaneous ANN (upper/lower panel). a) Spike trains of one/four neuron(s), b) instantaneous spiking frequency distribution at the indicated noise level, c) probability p for the instantaneous frequency to coincide with frequency of the perceived pitch f_p, for variable noise levels σ.

Fig. 3 shows measurements taken at f_c = 880 Hz, in the regime where the perceived pitch (measured as the first most prominent peak of the ISI distribution), is known to follow de Boer's first pitch shift rule [1]. In the absence of noise, high spontaneous neurons would quickly lock onto the signal, i.e., onto the modulation frequency (200 Hz, 5[ms]). It is only upon the addition of noise, that a distribution with a main peak at the perceived pitch f_p emerges. Sets of low-medium spontaneous neurons (that cannot directly encode f_p in their instantaneous frequencies), when driven by identical signals but independent noise, generate

an almost regular spike pattern, with a clear instantaneous frequency peak at locus of the perceived pitch f_p (the "volley principle" of auditory nerve coding). Fig. 3 demonstrates that this encoding of the perceived pitch in ANN spike rates bequests a nonzero amount of noise. Clearly, our simple median-based measure $p(\sigma)$ neither takes account of more global properties of the distribution, nor of how the pitch is finally extracted from the ANN (which may be the origin of the minor mismatch between the optimal noise in Table I vs. the optimal noise in Fig. 3), but otherwise our observations are very stable and consistent.

4. Discussion

From the peripheral hearing system, ever more details are known of the parts involved. How these parts functionally work together, however, has remained a challenge. Our full model of the peripheral hearing system is based on the principles of nonlinear physics and includes in a detailed manner the facts known from biology. Our model is in a sense minimal: the design of the cochlea, the inner hair cells, and the auditory nerve neurons, are extremely simple. Yet, our model not only reproduces all salient biological measurements to great accuracy, it also emphasizes the important role of synaptic noise in the transmission of salient hearing features, from the continuous basilar membrane motion to the discrete spiking world of the CNS. We demonstrated on the basis of physics that all nonlinear features of the auditory nerve can indeed be traced back to the active amplification process within the cochlea, a conclusion made previously on the basis of physiology [20].

A novel observation is that suprathreshold stochastic resonance seems to be necessary to enable the correct transition from IHC to ANN. In that respect we provide an important example of, and argument for, the omnipresence of noise in the nervous system. Audition is a particularly intriguing place for such an observation, as the mammalian hearing system is famous for its high temporal precision and reliability. In this sense, our approach opens the perspective upon a novel construction paradigm for high-precision information processing based on noisy elements, that circumvents bottlenecks encountered by current technology, particularly in chip design. Beyond this and offering new insights in hearing research, our model can serve as a template for faithfully transducing continuous into discrete-time systems, exceeding conventional high frequency sampling methods in efficacy and robustness. Due to its simple biological blueprint, it was simple to also realize the model in hardware, which yielded virtually coincident results.

References

[1] S. Martignoli and R. Stoop, Phys. Rev. Lett. **105**, 048101 (2010).

[2] A. Kern and R. Stoop, Phys. Rev. Lett. **91**, 128101 (2003).

[3] R. Stoop and A. Kern, Phys. Rev. Lett. **93**, 268103 (2004).

[4] Supplementary material for [1]. Available online at http://prl.aps.org/supplemental/PRL/v105/i4/e048101.

[5] R. Stoop, A. Kern, M.C. Goepfert, D. Smirnov, T. Dikanev, B.P. Bezrucko, Europ. Biophys. J. 35, 511-516 (2006).

[6] V.M. Eguíluz, M. Ospeck, Y. Choe, A.J. Hudspeth and M.O. Magnasco, Phys. Rev. Lett. **84**, 5232 (2000).

[7] E.A. Lopez-Poveda and A. Eustaquio-Martin, J. Assoc. Res. Otolaryngol. **7**, 218 (2006).

[8] M.C. Liberman, J. Acoustic. Soc. Am. **63**, 442 (1978).

[9] J.O. Pickles, *An Introduction to the Physiology of Hearing*, 3rd. Ed., Emerald Group, UK (2008).

[10] A.N. Temchin, N.C. Rich, and M.A. Ruggero, J. Neurophysiol. **100**, 2899 (2008).

[11] M. Müller, D. Robertson and G.K. Yates, Hear. Res. **55**, 50 (1991).

[12] R.F. Fox, I.R. Gatland, R. Roy, and G. Vemuri, Phys. Rev. A **38** (11), 5938 (1988).

[13] N.Y.-S. Kiang, T. Watanabe, C. Thomas, and L.F. Clark, *Discharge Patters of Single Fibers in the Cat's Auditory Nerve*, M.I.T. Research Monograph **35**, MIT Press, Boston (1965).

[14] C.D. Geisler, Brain Res. **212**, 198, (1981).

[15] N.F. Rulkov, I. Timofeev and M. Bazhenov, J. Comp. Neurosci. **17**, 2033 (2004).

[16] S.S. Narayan, A.N. Temchin, A. Recio, M.A. Ruggero, Science **282**, 1882–1884 (1998).

[17] E. de Boer, Nature **178**, 535 (1956).

[18] J.F. Schouten, R.J. Ritsma, and B.L. Cardozo, J. Acoust. Soc. Am. **34**, 1418 (1962).

[19] J.H.E. Cartwright, D.L. González and O. Piro, Phys. Rev. Lett. **82**, 5389 (1999).

[20] L. Robles and M.A. Ruggero, Physiological Reviews **81**, 1305 (2001).

[21] F. Jülicher, D. Andor, and T. Duke, Proc. Natl. Acad. Sci. U.S.A. **98**, 9080 (2001).